Journal of the Korean Nuclear Society
Volume 30, Number 6, pp.496~506, December 1998

Turbulent Natural Convection in a Hemispherical Geometry Containing Internal Heat Sources

Heedo Lee
Korea Power Engineering Company, Inc.
360-9, Mabuk-ri, Guseong-myun, Yongin-shi, Kyunggi-do, Korea 449-713

Goon-cherl Park
Seoul National University
San 56-1, Sillim-dong, Kwanak-gu, Seoul, Korea 151-742

(Received April 3, 1997)

Abstract

This paper deals with the computational modeling of buoyancy-driven turbulent heat transfer involving spatially uniform volumetric heat sources in semicircular geometry. The Launder & Sharma low-Reynolds number k-ε turbulence model without any modifications and the SIMPLER computational algorithm were used for the numerical modeling, which was incorporated into the new computer code CORE-TNC. This computer code was subsequently benchmarked with the Mini-ACOPO experimental data in the modified Rayleigh number range of $2\times10^{13}<Ra'<7\times10^{14}$.

The general trends of the velocity and temperature fields were well predicted by the model used, and the calculated isotherm patterns were found to be very similiar to those observed in previous experimental investigations. The deviation between the Mini-ACOPO experimental data and the corresponding numerical results obtained with CORE-TNC for the average Nusselt number was less than 30% using fine grid in the near-wall region and the three-point difference formula for the wall temperature gradient. With isothermal pool boundaries, heat was convected predominantly to the upper and adjacent lateral surfaces, and the bottom surface received smaller heat fluxes.

1. Introduction

During severe accidents in nuclear power plants, the molten core in the reactor vessel can relocate to the lower plenum, and form hemispherical shaped pools of molten reactor materials or corium. The high temperature pools of molten corium pose a threat to the structural integrity of the reactor vessel. The extent and urgency of this threat depend primarily upon the intensity of the internal heat sources and upon the consequent distribution and variation of the heat fluxes on the vessel walls in contact with the molten corium pools. The heat transfer inside the molten corium

can be characterized by the strong buoyancy-induced flows resulting from internal heating due to radioactive decay energy. The thermo-fluid dynamic characteristics of such flows depend very strongly on the thermal boundary conditions. The spatial and temporal variation of heat flux on the pool-wall interfaces or boundaries and the pool superheat characteristics depend strongly on the natural convection flow phenomena inside the molten pools[1]. In general, the natural convection heat transfer phenomena involving internal heat generation are adequately represented by the modified Rayleigh number, Ra′, which quantifies the internal heat source and hence the strength of the buoyancy forces.

During 1970-1982, Mayinger and his co-workers[2] carried out an experimental and theoretical research program involving natural convection heat transfer from a semicircular geometry. The investigations were carried out under the assumption of isothermal boundary conditions in the modified Rayleigh number range, $7\times10^{6}<Ra'<5\times10^{14}$. The computational model used in these analyses incorporated some concepts from forced convection, which are inconsistent with the basic physical mechanism of free convection where mean shear stresses are negligible. Also the model used by the Mayinger et al. extends the use of the effective turbulent thermal conductivity for the core flow region to the wall region. The predictions of the correlation for the downward heat transfer apper to be correct, but those for the upward heat transfer are apparently inaccurate.

Natural turbulent flows with internal heat sources inside semicircular cavities were also investigated theoretically and experimentally by Jahn & Reineke[3]. Both the temperature and velocity fields were measured in these experiments. Their investigations included numerical predictions of the velocity and temperature fields and comparisons with their corresponding experimental results. Although the numerical predictions show good agreement with the experimental results, the range of their investigations was limited to the low modified Rayleigh number range of $10^{9}<Ra'<10^{12}$.

Kelkar & Patankar[1] developed a mathematical model for accurate predictions of heat transfer in buoyancy-induced natural convection phenomena inside molten liquid pools with internal heat generation. They used the Jones & Launder low Reynolds number k-ε turbulence model, and concluded that incorporation of buoyancy correction and Yap correction in this model produced the best results for this core melt convection problem. However, their numerical investigations were not benchmarked with the corresponding experimental data. Instead, their numerical investigations were implemented using governing equations representing the conservation of the dimensionless quantities.

Dinh & Nourgaliev[4] developed a numerical model using the Chien low Reynolds number k-ε turbulence model for torispherical geometry, such as that of the Loviisa nuclear power plant. With the use of the Chien model without any modifications, the upward heat transfer rates were underestimated by a factor of about 2.5, while the downward heat flux predictions were slightly overestimated. They modified the turbulent viscosity coefficient for convection near the wall, and used a modified Prandtl number based on the local Richardson number. These authors were able to reproduce well the COPO test data by incorporating the preceding modification. However, they had considerable difficulty in benchmarking the NARAL computer code with the corresponding COPO experimental data.

As noted above, a literature survey of previous studies on the subject of the investigation reported here reveals the following : (i) There are scant or

limited experimental data for the hemispherical geometry in the high modified Rayleigh number range; (ii) there is no consensus for a reasonable numerical model benchmarked with the corresponding experimental data involving the low Reynolds number k-ε turbulence model. In view of this situation, the main subject and theme of this paper relates to the problem of a computational model for turbulent natural convection to evaluate the suitability of an appropriate model. The computational methodology used Launder & Sharma low-Reynolds number k-ε turbulence model[5] without any modifications. This methodology constitutes the basis for predicting the thermo-fluid dynamic characteristics of the two-dimensional buoyancy-induced convective flows. The control volume methodology of S. V. Patankar[6] was used in the computational algorithms for determining the variations of the thermal-hydraulic variables, including the velocity & temperature fields and the local & average heat transfer coefficients. The numerical investigations reported here also involved an analysis of important characteristics of buoyancy-induced turbulent flows, including the heat flux variation on the curved portion of the semicircular geometry and isothermal boundary conditions. A computer code, CORE-TNC, that incorporated the aforementioned numerical model and computational algorithm, was developed and the code results were benchmarked with the corresponding Mini-ACOPO experimental data[7]. The results obtained in this investigation can be used as a guide in the design of experiments for simulating buoyancy-induced turbulent flows of molten corium in a reactor vessel. Furthermore, these results can also be used to assess the thermal margin of a reactor vessel during severe accidents. In this connection, the surface heat flux variations and their maxima obtained in this investigation would be utilized for safety assessments in relation

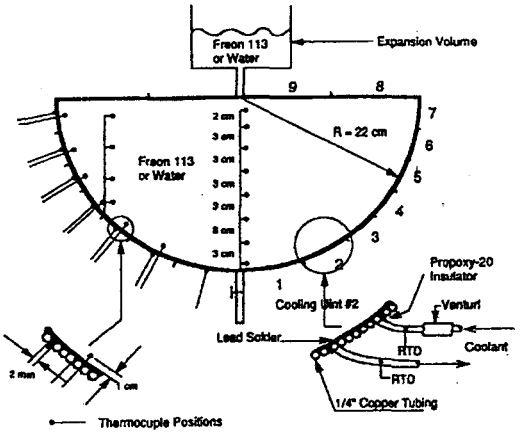

Fig. 1. Schematic of the Mini-ACOPO Experiment

to considerations for external flooding of the reactor vessel.

2. The Mini-ACOPO Experimental Facility

A schematic of the Mini-ACOPO test apparatus[7] is shown in Figure 1. This facility was constructed from 0.25 inch coiled copper tubing, brazed into shape, and filled in on the inside crevices with low melting solder to create smooth internal boundaries of a complete hemisphere (0.22m in diameter). The tubing was separated into nine separate circuits, each having its own inlet and outlet. The circuits were insulated from each other along all their interfacing areas. The wall region corresponding to each circuit can be heated or cooled to any desired temperature by simply connecting the circuit to an appropriate coolant bath. In this way, either isothermal conditions or any desired degree of initial stratification were created prior to the start of a cooldown transient. The Mini-ACOPO test apparatus was designed primarily for use with Freon-113, i.e., for a maximum pool temperature of about 40℃. Freon-113 was used for simulating molten corium in the Mini-ACOPO experimental

facility, to investigate the phenomenon of buoyancy driven natural convection with an internal heat source.

3. Mathematical Model

3.1. Governing Equations

It is assumed that the fluid flow is incompressible and satisfies the Boussinesq approximation. This Boussinesq approximation uses the following appropriate representation for the density, ρ, in the body force term:

$$\rho = \rho_o[1-\beta(T-T_{ref})] \tag{1}$$

The turbulent flow in the semicircular cavity is described by the Reynolds equations for mean flow. The Reynolds equations are obtained by time-averaging the instantaneous velocity components of the Navier-Stokes equations. The Reynolds stresses, $\overline{\rho u_i u_j}$, and the turbulent heat fluxes, $\overline{\rho u_j \theta}$, are given by the following equations, in accordance with the eddy viscosity model (EVM):

$$\overline{\rho u_i u_j} = \frac{2}{3}\delta_{ij}\rho k - \mu_t\left(\frac{\partial U_i}{\partial x_j} + \frac{\partial U_j}{\partial x_i}\right) \tag{2}$$

$$\overline{\rho u_j \theta} = -\frac{\mu_t}{\sigma_\theta}\frac{\partial \Theta}{\partial x_j} \tag{3}$$

If the Boussinesq approximation is inserted into the Navier-Stokes equations, a new unknown pressure p′ can be expressed by a combination of the hydrostatic pressure, p, and turbulent kinetic energy, k , as follows:

$$-\frac{\partial p'}{\partial x_i} = -\frac{\partial p}{\partial x_i} + \rho g_i - \frac{\partial}{\partial x_i}\left(\frac{2}{3}\rho k\right) \tag{4}$$

Using Cartesian tensor notation, the differential equations of the computational model employed here are given as follows:

Continuity equation:

$$\frac{\partial \rho}{\partial t} + \frac{\partial(\rho U_j)}{\partial x_j} = 0 \tag{5}$$

Momentum equation:

$$\frac{\partial}{\partial t}(\rho U_i) + \frac{\partial}{\partial x_j}(\rho U_j U_i) = -\frac{\partial p'}{\partial x_i} - \rho g_i \beta(\Theta - \Theta_{ref}) + \frac{\partial}{\partial x_j}\left[(\mu+\mu_t)\left(\frac{\partial U_i}{\partial x_j} + \frac{\partial U_j}{\partial x_i}\right)\right] \tag{6}$$

Turbulent (or eddy) viscosity:

$$\mu_t = C_\mu f_\mu \frac{\rho k^2}{\varepsilon} \tag{7}$$

Energy equation:

$$\frac{\partial}{\partial t}(\rho\Theta) + \frac{\partial}{\partial x_j}(\rho U_j \Theta) = \frac{\partial}{\partial x_j}\left[\left(\frac{\chi}{C_p} + \frac{\mu_t}{\sigma_\theta}\right)\frac{\partial \Theta}{\partial x_j}\right] + \frac{\dot{q}_{vol}}{C_p} \tag{8}$$

Turbulence kinetic energy equation:

$$\frac{\partial}{\partial t}(\rho k) + \frac{\partial}{\partial x_j}(\rho U_j k) = \frac{\partial}{\partial x_j}\left[\left(\mu + \frac{\mu_t}{\sigma_k}\right)\frac{\partial k}{\partial x_j}\right] + P_k + G_k - \rho(\tilde{\varepsilon} + D) \tag{9}$$

The turbulent kinetic energy is generated due to the interaction of the mean flow and the turbulent stresses. This interaction can be expressed via the scalar function P_k, which is defined as follows:

$$P_k = -\rho\,\overline{u_i u_j}\frac{\partial U_j}{\partial x_i} \tag{10}$$

The term G_k expresses the production of turbulence due to buoyancy, and using the eddy viscosity model, the following representation can be used for G_k:

$$G_k = -\beta\,\rho\,\overline{u_i\theta}\,g_i = \frac{\beta\mu_t}{\sigma_\theta} g_i \frac{\partial \Theta}{\partial x_i} \tag{11}$$

The additive term D in Equation (9) is used for improved representation of the near-wall behavior. The following expression for D is used in the current model, and is based on the Launder & Sharma turbulence model:

$$D = 2\nu \left(\frac{\partial\sqrt{k}}{\partial y}\right)^2 \quad (12)$$

Turbulence energy dissipation equation:

$$\frac{\partial}{\partial t}(\rho\bar{\varepsilon}) + \frac{\partial}{\partial x_j}(\rho U_j\bar{\varepsilon}) = \frac{\partial}{\partial x_j}\left[\left(\mu + \frac{\mu_t}{\sigma_\varepsilon}\right)\frac{\partial\bar{\varepsilon}}{\partial x_j}\right] + P_\varepsilon + G_\varepsilon - D_\varepsilon + E \quad (13)$$

$$P_\varepsilon = C_{1\varepsilon} f_1 \frac{\bar{\varepsilon}}{k} P_k \quad (14)$$

$$G_\varepsilon = (C_{1\varepsilon} f_1) C_{3\varepsilon} \left(\frac{\bar{\varepsilon}}{k}\right) G_k \quad (15)$$

$$D_\varepsilon = C_{2\varepsilon} f_2 \frac{\rho\bar{\varepsilon}^2}{k} \quad (16)$$

The following representation for the term E in Equation (13) is also based on the Launder & Sharma turbulence model:

$$G_\varepsilon = (C_{1\varepsilon} f_1) C_{3\varepsilon} \left(\frac{\bar{\varepsilon}}{k}\right) G_k \quad (17)$$

The turbulence Reynolds number, Ret, is defined as follows:

$$Re_t = \frac{k^2}{\nu\varepsilon} \quad (18)$$

The remaining empirical coefficients and functions in Equations (7) through (16), which are used in the Launder & Sharma low-Reynolds number k-ε turbulence model, are defined as follows:

$$C_\mu = 0.09,\ C_{1\varepsilon} = 1.44,\ C_{2\varepsilon} = 1.92,\ C_{3\varepsilon} = 1.0,\ \sigma_\theta = 0.9,\ \sigma_k = 1.0$$
$$\sigma_\varepsilon = 1.3,\ f_\mu = e^{\left(\frac{-3.4}{(1+\frac{Re_t}{50})^2}\right)},\ f_1 = 1.0,\ f_2 = 1 - 0.3e^{(-Re_t^2)} \quad (19)$$

Expressed in cylindrical polar coordinates, the general form of the scalar conservation laws, given above for the investigation presented here, can be written as follows:

$$\frac{\partial}{\partial t}(\rho\phi) + \frac{1}{r}\frac{\partial}{\partial r}(rV_r\rho\phi) + \frac{1}{r}\frac{\partial}{\partial\theta}(V_\theta\rho\phi) = \frac{1}{r}\frac{\partial}{\partial r}\left[\Gamma_\phi r\frac{\partial\phi}{\partial r}\right] + \frac{1}{r}\frac{\partial}{\partial\theta}\left[\Gamma_\phi r\frac{\partial\phi}{\partial\theta}\right] + S_\phi \quad (20)$$

The corresponding values of the diffusion coefficients Γ_ϕ and source terms S_ϕ for any general variable Φ are given in Table 1.

3.2. Solution Procedure

The set of differential equations for general variable Φ are solved by the control volume methodology[6]. The discretized equations are derived by integrating the differential equations over the control volume that surrounds the grid point under consideration. Values of the unknown discrete scalar variables, including pressure, temperature, and turbulence kinetic energy, are stored at each of the main grid points. The staggered grid is used for storing discrete velocity components. Thus, the control volumes for the velocities are staggered with respect to the main control volumes. The power law profile is used for obtaining fluxes across faces of the control volumes for the convective terms, and the integrated source term is linearized. The coupled discretized momentum, continuity, turbulence and energy equations are solved using the SIMPLER algorithm. The discretized equations for a given variable are solved using a line-by-line procedure coupled with a block-correction procedure.

Freon-113 was used for simulating molten corium in the Mini-ACOPO experimental facility, to investigate the phenomenon of buoyancy driven natural convection with an internal heat source. The material properties for this simulant are given as follows:

$$\rho_o\ (\mathrm{kg/m^3}) = 1550,\ \beta_o\ (/\ ^\circ\mathrm{K}) = 17\mathrm{X}10^{-4},$$
$$\mu\ (\mathrm{Kg/m\,sec}) = 0.64\mathrm{X}10^{-3},\ \nu\ (\mathrm{m^2/sec}) = 4.129\mathrm{X}10^{-7},$$
$$k\ (\mathrm{W/m^\circ K}) = 0.0741,\ c_p\ (\mathrm{J/Kg^\circ K}) = 962,$$
$$\alpha\ (\mathrm{m^2/sec}) = 0.5\mathrm{X}10^{-7},\ \mathrm{Pr}\ (\nu/\alpha) = 8.3 \quad (21)$$

Table 1. Expressions for the Diffusion Coefficients and Source Terms for Any Conserved General Property

Conservation Eq.	ϕ	Γ_ϕ	S_ϕ
Mass	1	0	0
Tangential Momentum	V_θ	$\mu + \mu_t$	$\frac{1}{r}\frac{\partial}{\partial r}(r\mu_{eff}(\frac{1}{r}\frac{\partial v_r}{\partial \theta} - \frac{v_\theta}{r}))$ $+\frac{1}{r}\frac{\partial}{\partial \theta}(\frac{\mu_{eff}}{r}(\frac{\partial V_\theta}{\partial \theta}+2V_r))$ $+\frac{\mu_{eff}}{r}(\frac{\partial V_\theta}{\partial r}+\frac{\partial V_r}{r\partial \theta}-\frac{V_\theta}{r})$ $-\frac{\rho V_\theta V_r}{r}-\frac{\partial P}{r\partial \theta}$
Radial Momentum	V_r	$\mu + \mu_t$	$\frac{1}{r}\frac{\partial}{\partial r}(r\mu_{eff}\frac{\partial v_r}{\partial r})$ $+\frac{1}{r}\frac{\partial}{\partial \theta}(r\mu_{eff}\frac{\partial}{\partial r}(\frac{V_\theta}{r}))$ $-\frac{2\mu_{eff}}{r^2}\frac{\partial V_\theta}{\partial \theta}-\frac{2\mu_{eff}}{r^2}V_r$ $+\frac{\rho V_\theta^2}{r}-\frac{\partial P}{\partial r}$
Energy	θ	$\frac{k}{C_p}+\frac{\mu_t}{\sigma_\theta}$	$\frac{q_{vol}}{C_p}$
Kinetic Energy	k	$\mu + \frac{\mu_t}{\sigma_k}$	$P_k + G_k - \rho\bar{\varepsilon} - \rho D$
Dissipation Rate	$\bar{\varepsilon}$	$\mu + \frac{\mu_t}{\sigma_\varepsilon}$	$P_\varepsilon + G_\varepsilon - D_\varepsilon + E$

The flat and curved walls of the semicircular cavity are assumed to be maintained at a constant temperature of 273° K. This corresponds to the molten corium liquidus temperature of about 2830° K[7].

The boundary conditions appropriate to the isothermal semicircular cavity are as follows:

$$\bar{U} = 0,\ T = T_w = 273°\,K,\ k=0,\ \bar{\varepsilon} = 0 \qquad (22)$$

The size of the entire computational grid used for the semi-circular cavity geometry is 80×60. For this geometry, the grid is defined along the θ-r directions. In turbulent fluid flows, the boundary layer is very thin; hence, the grid used in computations is very fine near the wall, in order to obtain accurate predictions of the flow field and the heat transfer characteristics. For example, the grid distribution near a wall at $\theta=0$ was specified according to the following equation:

$$X(i+1)=X(i)+1\times 10^{-9}\, i^{\,2.5} \qquad (23)$$

Together with the boundary conditions, a relaxation factor, β, is used to aid in the iterative solution of the discretized equation:

$$\phi = \beta\,\phi_{new} + (1-\beta)\,\phi_{old} \qquad (24)$$

Some underrelaxation factors were used to prevent divergence of the iteration process. The following β values were used for this purpose:0.5 to 0.3 for the velocity component; 0.995 to 0.5 for the temperature solution; 0.7 to 0.3 for k and ε.

At high Rayleigh numbers, the steady form of the discretized conservation equations exhibits oscillatory behavior. Therefore, the computations were carried out via a combination of steady and unsteady equations. The size of the time step was determined from a correlation developed by Kulacki and Emara[9]. This correlation was used for determining the Fourier number required for attaining the steady state value of the Nusselt number for natural convection in internally heated fluid layers. This correlation can be expressed as follows:

$$Fo_{max} = 11.577(\Delta Ra)^{-0.213} \quad (25)$$

$$Fo_{max} = \frac{\alpha t_{max}}{L^2} \quad (26)$$

$$Fo_{max}=7.97\times10^{-3},\ t_{max}=7717 \text{ sec for } Ra' = 7\times10^{14} \quad (27)$$

In Equations (25) through (27), t_{max} is the time required to reach steady-state conditions for maximum temperature difference. Since unsteady computations are initiated after performing a large number of iterations for the steady state form of the equations, the time scale for unsteady computations is estimated as $1/500^{th}$ of the Fourier number predicted from Equation (26).

3.3. Nusselt Number

From thermal engineering viewpoint, the most important characteristic of the flow is the rate of heat transfer across the cavity. The average Nusselt number at the surface can be determined from the following relations:

$$\overline{q''} = \frac{\int(-k\nabla T)\,dA}{\int dA} \quad (28)$$

$$\overline{Nu} = \frac{\overline{h}\,R_o}{k} = \frac{\overline{q''}\,R_o}{k(T_{max}-T_w)} \quad (29)$$

Very careful consideration was given when the bounrary conditions were treated. The reason is that half control volumes are employed near the boundaries, and the interface is located at the boundary, thus setting the thickness of the half control volumes equal to zero. Boundary treatment techniques such as the two-point and three-point difference formulas were considered. The three-point difference formula is recommended here for resolving the wall temperature gradient. A brief account of this numerical differencing method follows[10]:

$$-k\frac{dT}{dy} = -\frac{4}{3}\frac{k_2}{(y_2-y_1)}(T_2-T_1)+\frac{1}{3}\left[\frac{\delta y_{e-}}{k_2}+\frac{\delta y_{e+}}{k_3}\right]^{-1}(T_3-T_2) \quad (30)$$

Subscript 1 denotes the boundary surface, and subscripts 2 and 3 denote the near-wall grid points. δy_{e-} and δy_{e+} denote the distances from grid points 2 and 3, respectively to the interface.

4. Results and Discussion

The variation of time-averaged Nusselt numbers with modified Rayleigh numbers, Ra′, is shown in Figure 2 and Figure 3 for the curved surface and the upper flat surface, respectively. The deviation between the Mini-ACOPO experimental data and the corresponding

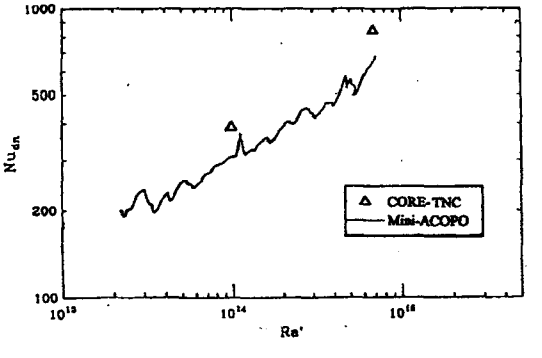

Fig. 2. Nusselt Number, Nu_{dn}, Variation with Modified Rayleigh Number, Ra′ for Downward Heat Transfer

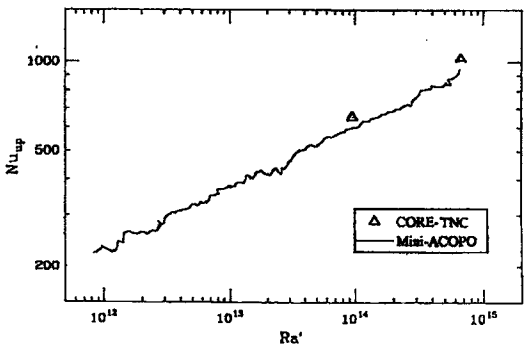

Fig. 3. Nusselt Number, Nu_{up}, Variation with Modified Rayleigh Rumber, Ra′ for Upward Heat Transfer

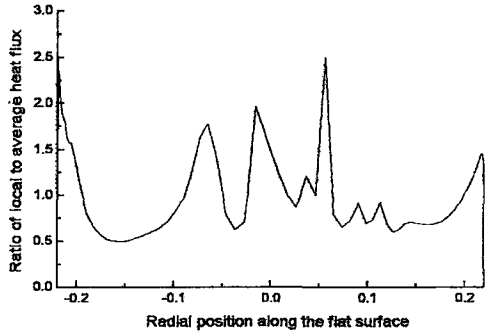

Fig. 4. Local Heat Flux Variation with Radial Location Along the Upper Flat Surface for Ra′ =7 × 10^{14} and Pr = 8.3

numerical results from the CORE-TNC code output for the average Nusselt number, was less than 30%.

The buoyant flow pushes the hot fluid into the upper region of the semicircular cavity, causing the generated heat to be transferred mostly over the flat surface and the upper regions of the curved surface as shown in Figures 4 and 5. Thus, with reference to the lower right quadrant of the circle, the heat transfer rate on the curved surface is biased toward the upper portion($0<\theta<45$) in comparison to the lower part($45<\theta<90$), as shown in Figure 5. On the other hand, no systematic variation or trend

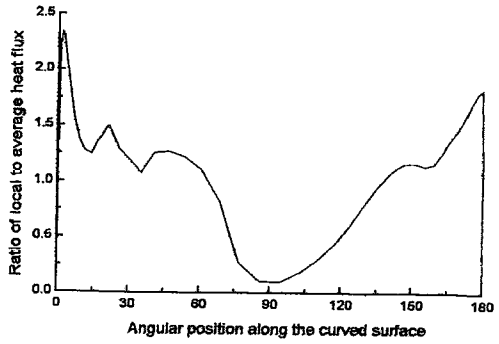

Fig. 5. Local Heat Flux Distribution with Angular Variation Along the Curved Surface for Ra′ =7 × 10^{14} and Pr = 8.3

toward peaking of heat fluxes was found along the horizontal upper boundary, as can be seen from Figure 4.

Figure 6 shows the corresponding flow patterns during one period of oscillation. The computations show that the regions of laminar and turbulent flow coexist due to thermal stratification, as is shown in Figures 7 through 9. The calculated isotherm patterns are very similiar to those observed experimentally for semicircular cavities by Jahn & Reineke[3], and by Mayinger et al[2]. The lower part of the curved surface is well stratified, while the upper part is characterized by time-varying convection eddies. These eddies, formed underneath the flat surface on top, grow and shrink in size and cause a strong flow below the flat surface. The constantly evolving eddies also have a pronounced effect on the temperature field. The eddy flow underneath the flat surface enhances the heat transfer to the top surface.

The computed turbulent viscosity, turbulent kinetic energy, kinetic energy dissipation, and turbulence Reynolds number are shown in Figures 10 through 13, respectively, for Ra′ = 7 × 10^{14} and Pr = 8.3.

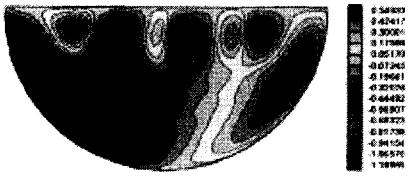

t = 0.00sec

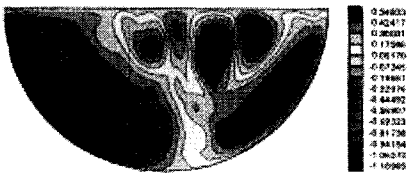

t = 0.29sec

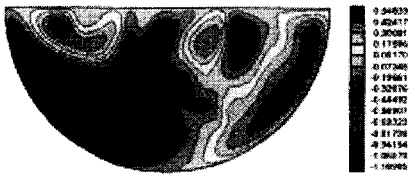

t = 0.71sec

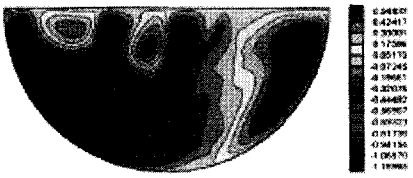

t = 1.13sec

Fig. 6. Flow Patterns During one Period of Oscillation for Ra′ =7 × 10^{14} and Pr = 8.3

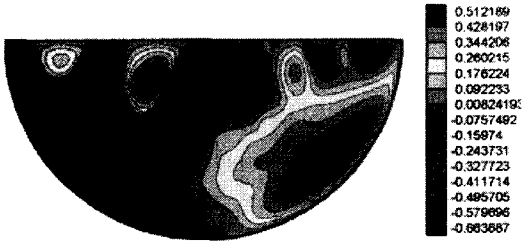

Fig. 7. Turbulent Mean flow Streamlines for Ra′ =7 × 10^{14} and Pr = 8.3

Fig. 9. Temperature Field for Ra′ =7 × 10^{14} and Pr = 8.3

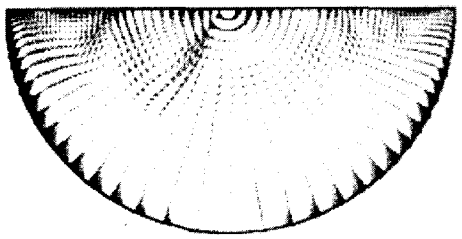

Fig. 8. Turbulent Mean flow Velocity Fields for Ra′ =7 × 10^{14} and Pr = 8.3

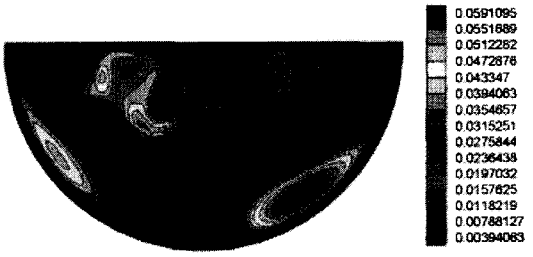

Fig. 10. Turbulent Viscosity for Ra′ =7 × 10^{14} and Pr = 8.3

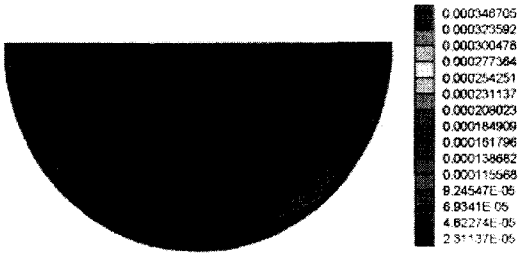

Fig. 11. Turbulent Kinetic Energy for Ra′ =7 × 10^{14} and Pr = 8.3

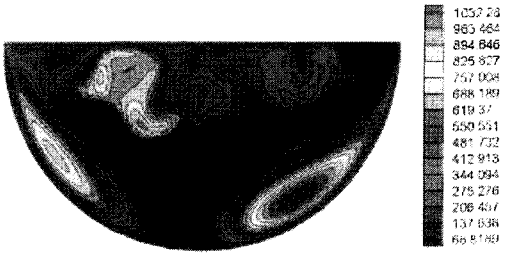

Fig. 13. Turbulence Reynolds Number for Ra′ =7 × 10^{14} and Pr = 8.3

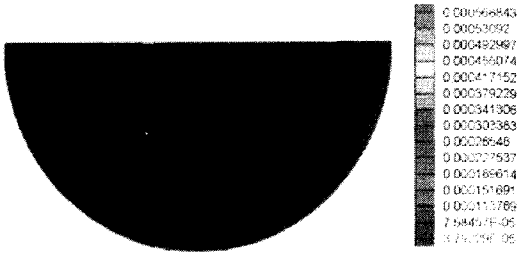

Fig. 12. Turbulence Energy Dissipation for Ra′ =7 × 10^{14} and Pr = 8.3

5. Conclusions

This paper presents a computational method that was used to obtain solutions of the buoyancy-driven turbulent heat transfer phenomena for semicircular geometry, with uniformly distributed volumetric heat sources. Freon-113 was used to simulate the buoyancy-driven natural convection phenomena. The modified Ra′ number range examined in this investigation varied between 2×10^{13} and 7×10^{14}. The Launder-Sharma low-Reynolds number k-ε turbulence model and the SIMPLER algorithm were utilized to predict heat transfer in turbulent flow, including determination of the velocity field and the temperature distribution. The calculated isotherm patterns were found to be very similiar to those observed in the experimental investigations by Jahn & Reineke, and by Mayinger et al. for semicircular cavities. The deviation between the Mini-ACOPO experimental data and the corresponding numerical results from the CORE-TNC code output was less than 30% for the average Nusselt number. No systematic variation or trend toward peaking of heat fluxes was found along the horizontal upper boundary. On the other hand, the heat transfer rate is biased toward the upper portion of the curved boundary. With isothermal pool boundaries, heat was convected predominantly to the upper flat surface and to adjacent parts of the lateral surfaces, while the bottom portion of the curved surface received smaller heat fluxes.

It is concluded that the reduced deviation in comparisons between the CORE-TNC model and the Mini-ACOPO experimental data are principally due to an improved representation for the near-wall behavior in the CORE-TNC model. Future modeling is expected to concentrate on further refinement of the near-wall model representation.

Acknowledgement

The authors wish to acknowledge valuable comments from Professor T. G. Theofanous and Professor S. V. Patankar in the preparation of the manuscript.

References

1. Kelkar K. M. , Khankari K. K. , and Patankar S. V. , "Computational Modeling of Turbulent Natural Convection in Flows simulating Reactor Core Melt" , Innovative Research Inc., Final Report Submitted to SNL, Albuquerque, NM 87115, December (1993).
2. Kulacki F. A. , "Review and Evaluation of Examination of Thermohydraulic Processes and Heat Transfer in a Core Melt,, by Mayinger, Jahn, Reineke, and Steinbrenner,, Letter Report prepared for the U.S. Nuclear Regulatory Commission under contract AT (49-24)-0149, March 31, (1976).
3. Jahn M. and Reineke H. H., "Free Convection Heat Transfer with Internal Heat Sources - Calculations and Measurements,, Proceedings of the 5th International Heat Transfer Conference, NC2.8, Tokyo, Japan, Sept. 3-7, (1974).
4. Dinh T. N. and Nourgaliev R. R. , "On Turbulence Modeling for Large Volumetrically Heated Liquid Pools", Submitted for Publication in Nucl. Eng. Deg, (1995).
5. Launder B. E. and Sharma B. I., "Application of the Energy-Dissipation Model of Turbulence to the Calculation of Flow Near a Spinning Disc., Letters in Heat and Mass Transfer, Vol. 1, pp.131-138, (1974).
6. Patankar S. V. , "Numerical Heat Transfer and Fluid Flow", Hemisphere, New York, (1980).
7. Theofanous T. G. , Liu C. , Angelini S. , Kymalainen O. , Tuomisto H. and Additon S. , "In-vessel Coolability and Retention of a Core Melt", DOE/ID-10460, Volume I and II, July (1995).
8. Patel V. C. , Rodi W. , and Scheuerer G. , "Turbulence Models for Near-Wall and Low Reynolds Number Flows: A Review,, AIAA Journal, Vol.23, No.9, (1985).
9. Kulacki F. A. and Emara A. A. , "Steady and Transient Thermal Convection in a Fluid Layer with Uniform Volumetric Energy Sources,, Journal of Fluid Mechanics, Vol.83, part 2, pp. 375-395, (1977).
10. Patankar S. V. , "Computation of Conduction and Duct Flow Heat Transfer", Innovative Research, Inc., (1991).